INSTANTANEOUS PHASE VARIATION FOR SEISMIC VELOCITY MONITORING FROM AMBIENT NOISE AT THE EXPLORATION SCALE.

Margherita Corciulo[(1)], Philippe Roux[(1)], Michel Campillo[(1)] and Dominique Dubucq[(2)]

Right Running Head: Passive monitoring from IPV estimation

[(1)] Institut des Sciences de la Terre, Université Grenoble 1, CNRS UMR 5275, Grenoble, France.

E-mail: margherita.corciulo@obs.ujf-grenoble.fr; philippe.roux@obs.ujf-grenoble.fr; michel.campillo@obs.ujf-grenoble.fr.

[(2)] TOTAL, Centre Scientifique et Technique Jean-Féger, Pau, France.

E-mail: dominique.dubucq@total.com.

Date of submission: 27 September 2011

bstract

Recent studies in geophysics have investigated the use of seismic-noise correlations to measure weak-velocity variations from seismic-noise recordings. However, classically, the existing algorithms used to monitor medium velocities need extensive efforts in terms of computation time. This implies that these techniques are not appropriate at smaller scales in an exploration context when continuous datasets on dense arrays of sensors have to be analysed. In the present study, we apply a faster technique that allows the monitoring of small velocity changes from the instantaneous phase measurement of the seismic-noise cross-correlation functions. We perform comparisons with existing algorithms using synthetic signals. The results we have obtained for a real dataset show that the statistical distribution of the velocity-change estimates provides reliable measurements, despite the low signal-to-noise ratio obtained from the noise-correlation process.

Introduction

Passive imaging techniques that use ambient-noise data are based on reconstructions of the Green's function by cross-correlation of data acquired at two locations, which provides the expression of the wave propagation from a virtual source at one station as recorded at the other (Weaver and Lobkis, 2001; Shapiro and Campillo, 2004; Snieder, 2007). This property has been extensively used to perform noise-based surface-wave tomography at observation scales that range from hundreds of kilometers (Shapiro et al., 2005; Yao et al., 2006) down to a few kilometers (Roux et al., 2011).

In addition to surface-wave tomography, passive processing based on seismic-noise cross-correlation is of growing interest for the monitoring of temporal changes of complex structures, such as volcanoes or fault zones at the geophysics scale (Sabra et al., 2006; Sens-Schönfelder and Wegler, 2006; Hadziioannou et al., 2009; Brenguier et al., 2008, 2011).

The recent passive monitoring investigations find their roots in the early work of Poupinet et al. (1984), who proposed the measurement of small velocity variations using the direct arrivals of earthquake multiplets. This technique, which was originally called doublet technique in seismology, computes the time delay for two signals that originate from the same location and that are acquired at different times at the same position. Time delay was computed as the estimation of the phase shift measured in the frequency domain for short time windows selected in the coda of the recorded signals. Indeed, small velocity changes that have no detectable influence on the direct arrivals are amplified by multiple scattering and can thus be readily observed in the coda. Later on, Coda Wave Interferometry (CWI) revisited the doublet technique, from repetitive sources in geophysics at higher frequencies and on smaller scales (Snieder et al., 2002;

Grêt et al., 2005; Snieder et al., 2006). To estimate the accuracy of the velocity variation estimation, these techniques use the correlation coefficient, which provides a measure of the similarity of the two time-windowed signals.

The new idea that arose from passive interferometry after 2005 was to replace the use of repetitive sources by the computation of the seismic-noise correlation function between two sensors. Indeed, with the last decade seeing the development of continuous recordings on large seismic arrays, different sets of two-point cross-correlation functions (CCFs) of ambient noise records have become available at repetitive time intervals. Interestingly enough, through laboratory experiments (Hadziioannou et al., 2009), it has even been shown that the monitoring of relative velocity variations through the collection of CCFs is possible even when the exact Green's function is not retrieved from the correlation process. In other words, it is now acknowledged that the requirements to perform passive monitoring are less restrictive than for noise-based tomography.

In the last few years, two techniques have been applied to perform passive monitoring from the noise-based CCFs. Following its original application to active sources, the doublet technique was applied to a collection of short time windows selected in the coda of the CCFs at times where the correlation coefficient between the two time-gated signals is sufficiently high (Brenguier et al., 2008, 2011).

Similarly, small velocity variations can also be measured using the stretching technique, which consists of distorting the current CCF to obtain the best coherency with the reference CCF (Sens-Schönfelder and Wegler, 2006; Hadziioannou et al., 2009). This technique is based on the time-domain interpolation of the whole waveform on a modified version of the time axis that is either stretched or compressed, according to an eventual increase or decrease in the medium velocity. The optimal stretching

coefficient is obtained when the correlation coefficient between the reference and the distorted CCFs reaches a maximum.

When performed on noise-correlated data, the doublet and stretching techniques capitalize on the (multi)scattered signals that have extensively explored the propagation medium. However, it should be noted that both of these techniques require extensive efforts in terms of computation time. The doublet technique needs most of this time for the appropriate choice of the short time windows where the phase variation is calculated, while the stretching method needs to explore all of the possible stretching coefficients. Finally, the heavy computation time makes the doublet and stretching techniques quite inappropriate when dealing with continuous datasets that include a very large number of stations, as is often the case at the exploration scale.

To image and monitor reservoirs in exploration geophysics, the virtual-source method has been successfully applied using controlled-source datasets (Bakulin et al., 2007; Korneev et al., 2008). This technique implies the use of sensors located underneath complicated overburdens, to avoid transmission effects at the near surface and to focus on reflections from deeper targets. This technique is limited by the presence of high-amplitude ghost signals that are associated with the source–receiver separation, and by the difficulty of deploying several sensors in multiple boreholes to monitor a large area.

Seismic interferometry has also been used in exploration geophysics since the early 2000's. A study proposed by Schuster et al. (2004) showed that seismic imaging using cross-correlated data obtained from a collection of sources can offer new tools to migrate multiple waves, such as peg-leg multiples from common depth point data. However severe migration artifacts were retrieved when virtual multiples were present in the correlated data.

More recently, a study presented by Draganov et al. (2007) successfully used ambient-noise data that was acquired along a single line to isolate P-wave reflections. Their noise-correlation results were successfully compared to results obtained from an active seismic experiment that was available for the same line, and that showed the same body-wave reflections. This study was pioneering, in the sense that most noise-based passive processing had previously been limited to surface-wave extraction, which classically dominates the seismic-noise records. Indeed, the analysis of active and passive data acquired at the exploration scale classically shows that the seismic noise is dominated by low-frequency surface waves, in a frequency band outside the active-source frequencies that excite body waves. Passive and active datasets, with their different wave types, can then be used together to obtain complementary information about the properties of the medium.

Finally, it should also be mentioned that passive seismic processing has been used to continuously monitor ocean-bottom seismic clock-time drift during acquisition surveys (Hatchell and Mehta, 2010), following earlier studies on array synchronization in underwater acoustics (Sabra et al., 2005a) and seismology (Stehly et al., 2007).

In conclusion, there has been a growing interest in the development of passive methodologies at the exploration scale over the last decade. The use of dense arrays and the trend towards continuous recordings lead to the collection of huge datasets in the context of exploration geophysics. The need for quasi-real-time passive monitoring is a strong motivation for the development of new and faster processing algorithms.

With this goal in mind, the present study demonstrates a technique for passive monitoring that is based on the measurement of the instantaneous phase of noise-correlated signals. This instantaneous phase variation (IPV) technique aims to combine

the advantages of the doublet and stretching methods, while proposing a much faster measurement of the velocity change.

The description of the IPV technique is presented in the next section, before its comparison with the doublet and stretching techniques using synthetic data. Focusing on low-frequency surface waves, the IPV technique is used to perform passive seismic monitoring analysis using a continuous seismic-noise dataset that was acquired over a five-day period above an exploration field.

Instantaneous phase variation

The IPV technique is based on the estimation of the local phase shift for two CCFs computed for a station pair at two different acquisition times. The instantaneous phase is calculated from the time-domain analytic signal $S(t)$, as defined by Gabor (1946):

$$S(t) = s(t) + iH[s(t)] = A(t)\exp(i\varphi(t)) \quad (1)$$

where $s(t)$ is the cross-correlated time series, and H is the Hilbert transform (Hilbert, 1900). $S(t)$ is a complex signal from which the instantaneous amplitude $A(t)$ and phase $\varphi(t)$ can be separated (Bracewell, 1965). As the Hilbert transform is classically used for demodulation of narrow-band signals, the instantaneous phase $\varphi(t)$ is calculated on finite-bandwidth pre-filtered signals. Note that Schimmel et al. (2011) also used instantaneous phase coherence as a way to improve Green's function estimations from noise-correlation processes.

For a given station pair, we assume now that two CCFs, $s_1(t)$ and $s_2(t)$, are calculated for a given frequency bandwidth (centered at frequency ω) for two ambient-noise time windows that are selected around the acquisition times t_1 and t_2, respectively. From the analytic signals $S_1(t)$ and $S_2(t)$ obtained from equation (1), the instantaneous phase shift $\Delta\varphi(t)$ between the two CCFs is defined as:

$$\Delta\varphi(t) = \varphi_1(t) - \varphi_2(t) = \omega t \frac{dV}{V} \qquad (2)$$

As the noise-based CCF between a station pair is assumed to provide the travel times of both direct and scattered waves (Weaver and Lobkis, 2004; Roux et al., 2005; Snieder, 2007), $\Delta\varphi(t)$ is linearly related to the velocity variation dV/V of the medium between the two different realizations at t_1 and t_2. The estimation of dV/V is then performed from linear regression applied to $\Delta\varphi(t)$.

As velocity variations affect late arrivals more than early arrivals, as the former travel through the medium for longer time, the accuracy of the linear regression performed on $\Delta\varphi(t)$ increases with time. However, late arrivals in the CCF also suffer from lower signal-to-noise ratios (SNRs), which results in phase uncertainties that are seen as 2π phase jumps in $\Delta\varphi(t)$. As a consequence, a balance has to be found between the slope accuracy provided by the late arrivals and the slope robustness obtained from the higher-amplitude early arrivals in the CCF.

Application to a synthetic dataset

To assess the robustness and accuracy of the IPV technique for the measurement of weak velocity variations, a quantitative comparison was performed with the doublet and stretching techniques. This comparison was performed using a synthetic dataset that was designed to represent the frequency–time characteristics of the CCFs measured with the dataset acquired in the context of exploration geophysics, and as described in the next section.

The purpose of this numerical test is to evaluate the relative statistical performances of these three monitoring techniques (doublet, stretching and IPV) in the presence of noise. With this goal in mind, a normalized random-like signal that was filtered in the [2-5 Hz] frequency band was first synthesized (Figure 1a). This reference signal mimics a reference noise-based CCF between -2 s and +2 s. The different wavelets in Figure 1a would correspond to the unpredictable superposition of direct and/or scattered surface waves extracted from the ambient seismic noise, as classically seen with real data when the noise source is not homogeneously distributed. For the sake of simplicity, no amplitude damping, that corresponds to attenuation and geometrical spreading, was applied to the signal.

In a second step, the reference CCF was stretched using a given value of velocity change $\varepsilon = dV/V$ (Figure 1b, red signal). Random noise generated in the same frequency band was then added, to pollute both the reference and the stretched CCFs (Figure 1c, d, gray signals). Finally, the doublet, stretching and IPV techniques were used to produce an estimate of dV/V between the “noise + reference” CCF and the “noise + stretched” CCF, and compare this to its expected value ε.

To perform a statistical analysis of the dV/V estimates, the same velocity change ε was used to stretch one thousand different synthetic realizations of the reference CCF. Figure 2 shows the one thousand dV/V estimates obtained using SNR = 5 and SNR =

100 for a set of ε values from 0.5×10^{-3} to 5.0×10^{-3}. A first look at these data shows that the three monitoring techniques are equally sensitive to the SNR. For each ε (Figure 2, X axis), the dV/V estimates (Figure 2, Y axis) have a much larger statistical dispersion for SNR = 5 than for SNR = 100. Among these three techniques, the stretching method appears to perform better for the recovery of the ε value, which was expected as stretching was used to distort the reference CCF. A finer look at the dV/V estimates also reveals a potential bias of the average IPV results for ε larger than 4.0×10^{-3} (Figure 2a, b, black crosses). This underestimation of the average dV/V is due to the 2π phase shifts that are observed between the two instantaneous phase measurements when (1) the amplitude of the CCF goes to zero or (2) the reference and stretched CCFs become too different at the later arrival times.

A first conclusion of this numerical test is that an unbiased estimation of ε is difficult at low SNR for a limited number of CCFs. The advantage of exploration-scale data lies in the large number N of stations deployed during the acquisitions, which results in a tremendous number of CCFs, $N(N-1)/2$, from which monitoring studies can be performed. Indeed, when a large set of reference CCFs is used, the Gaussian distribution of the estimated dV/V allows for statistical fitting of the results, from which an unbiased estimation of ε can be retrieved, regardless of the SNRs (Figure 3a).

To determine the fastest of these methodologies, the computation times necessary to compute the whole set of estimated dV/V values were compared across these doublet, stretching and IPV techniques. Table 1 summarizes the absolute and normalized computation times obtained for [-2s, 2s] duration CCFs analyzed with SNR = 5. The computation times were calculated on the same computing platform, and only the relative values between the different techniques should be considered here. There are large differences across the three monitoring algorithms. Compared to the doublet

and stretching techniques, the IPV benefits from fast algorithms that are developed for the Hilbert transform computation and the simplicity of the direct measurement of the instantaneous phase. As expected from the computational complexity, the IPV technique appears to be the fastest, while the slowest is the doublet technique.

Passive seismic monitoring through IPV applied at the exploration scale

The IPV technique was applied to seismic-noise data recorded on a dense network of geophones deployed for imaging and monitoring purposes in the context of exploration geophysics.

Five days of continuous ambient seismic noise were acquired for a total of 397 stations laid out on 13 lines on a 0.8-km-sided, squared array that was located above an oil and gas exploration field (Figure 4). The stations were equipped with 10-Hz vertical-component geophones buried in 9-m-deep holes. The data that were originally sampled at 1000 Hz were band-pass filtered between 2 Hz and 5 Hz before computing the CCF, using 10-min-long time series (Figure 5).

Note that the CCF is not symmetric with respect to the zero time of the correlation, which is the signature of anisotropic distribution of the noise sources. As such, this means that the surface-wave reconstruction through the correlation process is probably biased. However, as demonstrated by Hadziioannou et al. (2009), passive monitoring can still be performed efficiently with a poorly reconstructed Green's function as long as the noise source remains unchanged during the acquisition period.

The choice of the low-frequency interval [2-5 Hz] was motivated by the observation of both direct and scattered surface waves in the CCF, as coherent wavelets expand over more than 2 s on both the positive and negative time axis when the direct

arrival is expected at ~0.1 s (Figure 5b). At higher frequencies (e.g. above 10 Hz), although scattered surface waves can still be present in the CCF, the strong attenuation in the medium strengthens the spatial coherence decay with the inter-station distance, which finally limits the number of sensor pairs on which the monitoring algorithm can be performed.

Figure 6b shows the time evolution of the CCFs for the station pair #125 and #128 (chosen arbitrarily; see Figure 4, yellow squares) over the five recording days. The early arrivals that correspond to direct waves are very coherent over the whole of the 5-day recording except for one time interval during the first day (around acquisition time = 18 h) during which a sudden change in the direction of the dominant noise source was observed, as confirmed by a beamforming analysis. Late arrivals are also evident showing clear coherent phases throughout the CCFs, which extend to time lags of up to ~3 s (Figure 6a, c). As 10-Hz geophones were used to record the ambient noise, it can be noted that high-amplitude CCFs can be extracted at low frequencies.

The size of the recording dataset made the IPV technique a good candidate to evaluate the relative velocity changes in the medium over reasonable computation times. Indeed, considering all of the station pairs among the 200 geophones arbitrarily chosen (Figure 4, red spots) and the remaining 397 geophones, a total of 79,400 station pairs were processed. As these data were continuously acquired over five days, and as 10-min-long time series were used to compute each CCF, a total of about 700 time windows were available, which corresponds to a total of about 56×10^6 CCF comparisons made on this dataset.

As small velocity changes were expected, the reference CCF was computed as the 5-day stack of all of the 10-min-averaged CCFs for each station pair. Only the [-2s, +2s] time interval of the CCF was kept for monitoring purposes. Although the synthetic

test showed that statistical analysis of the estimated dV/V on a large set of CCFs allows the SNR constraint to be released, a 1-h average on six consecutive CCFs was performed to improve the SNR. Each 1-h-averaged CCF was then compared to the reference CCF with a sliding window of 10 min, which preserves good time resolution over the five recording days.

A Gaussian distribution was used to fit the dispersion of the IPV-estimated dV/V results. Examples of actual measures are presented in Figure 3b. At this stage, the results were discarded if the variance of the Gaussian distribution was larger than 1%. This threshold depends on the coherence level of the CCFs and the number of geophones on the array. This first step of the processing provides detection of time intervals when no data were available on a large set of geophones (Figure 7a, blue time intervals). Finally, both the mean and the standard deviation of the Gaussian fit were kept as the dV/V estimate and the error bars, respectively.

The 5-day monitoring results are shown in Figure 7. The temporal evolution of the average dV/V is plotted in Figure 7c. The standard deviation σ of the Gaussian fit is shown in Figure 7b. As shown in Figure 2, the σ is a signature of the SNR of the CCFs. Using the synthetic tests shown before, an average value $\langle\sigma\rangle = 5\times10^{-3}$ (Figure 7b) would correspond to a SNR ~2.8, which is in agreement with the experimental results. Indeed, the residual standard deviation δn of the ambient noise CCF varies as the inverse of the time-bandwidth product of the selected noise interval [Sabra et al., 2005b]:

$$\delta n = \frac{1}{\sqrt{2BT}} = 6.8\times10^{-3} \qquad (3)$$

with T = 1 h and B = 3 Hz for the present dataset. On the other hand, the average amplitude A = 1.88 $\times 10^{-2}$ of the CCFs can be measured as the square root of the average intensity over the [-2s, +2s] time interval used for the monitoring. It is interesting to note that this estimation of the SNR = A/δn = 2.76 of the cross-correlation process is consistent with the SNR prediction from the Gaussian fit of the estimated dV/V through the monitoring algorithm (Figure 8). Note that similar data for the dV/V error estimation measured from the noise correlation coefficient for the stretching method were presented in a recent report by Weaver et al. (2011).

From Figure 7, we can see that the time evolution of the estimated dV/V and the width σ of the Gaussian distribution are generally not correlated. This is particularly visible between Day 1 and Day 2, where the increase in dV/V corresponds to a stable value of σ. Sharp and fast variations of dV/V can also be noted starting from midday of Day 3.

As usual, with passive monitoring studies at larger scales (Brenguier et al., 2008, 2011), it can be asked whether the velocity variations are due to an actual change in the elastic properties of the medium, or to a change in the noise-source distribution. We noted for the example shown in Figure 6 that the correlation coefficient between the time-evolving CCFs and the reference was quite stable over the five recording days. This stability of the wave shapes is an indication of the noise source steadiness. We also notice that the sudden change in the ballistic arrivals of the CCF during the first day (around acquisition time = 18 h, see Fig. 6b) does not correlate with a change in dV/V. Actually, the IPV technique only uses the phase of the CCF and not the amplitude information associated to the direct or scattered waves. So, despite the fact the ballistic part of the CCF is modified by the sudden change in the local noise source directivity, the scattered part of each CCF stays stable enough to provide a stable dV/V. Note,

however, that the standard deviation σ looks affected by the source directivity change during day 1 which means that part of the CCFs are probably more sensitive to this source directivity change than others.

This further confirms that the velocity variations seen in the last part of the experiment should originate from a slight change in the medium properties.

In the [2-5 Hz] frequency bandwidth, beamforming analysis performed on the same dataset revealed that the seismic-noise recordings were dominated by surface waves due to human activity. More precisely, the dominant noise source was identified as the nearby extraction platform at the North-East of the array deployment. Through beamforming, an average surface-wave phase velocity was measured at around 300 m/s. Assuming that the scattered waves in the noise correlation function are also dominated by surface-wave components, then the relevant wavelength is on the order of 100 m for a penetration depth (or a sensitivity at depth) that is classically of the same order. Although conversions from surface to body waves, and the reverse, are expected, the predominance of surface-wave energy leads to the consideration that our measurements have the sensitivity of surface waves. The velocity change measured through IPV in the present study might then not be connected directly with the gas-extraction process for an injection well and a reservoir at a depth of 400 m. However, significant changes might also occur in the overburden above the injector. Finally, even though the dV/V estimation only corresponds to the shallow subsurface fluctuations, this statics correction should be taken into account to provide unbiased images of the time-evolution of the gas reservoir through classical active seismic-exploration techniques.

Unfortunately, no independent measurements of the medium properties were made during the course of these recordings. As a separate analysis, the micro-seismicity

event rate was inferred at different times from the seismic data above 30 Hz, but there was no evidence of any correlation with the dV/V time evolution.

Conclusions

The use of seismic-noise data to perform passive monitoring in exploration geophysics is still under debate. The methodological aspects presented in the present study provide some new ingredients here. The use of (1) continuous recordings on a very dense seismic network, and (2) instantaneous phase measurements of the noise-based correlation functions through the Hilbert transform makes the instantaneous phase variation (IPV) technique a viable method for passive monitoring of velocity variations in the context of exploration geophysics.

In this way, large passive datasets can be investigated through statistical analysis, to reduce the uncertainties of the dV/V estimation.

Compared to other passive monitoring techniques, the IPV algorithm gives satisfactory results with time-limited cross-correlation functions, as seen in exploration geophysics where strong attenuation is common at the subsurface. Similarly, the IPV monitoring method performs better when small velocity changes are observed, which is likely to occur with an oil field or a gas reservoir.

Finally, the IPV shows interesting perspectives for passive monitoring that allows a quasi-real-time analysis of the subsurface elastic properties on any large dataset. Future studies should investigate the possibility of gathering spatial information by the monitoring of different sub-arrays above a reservoir or by performing the monitoring algorithm over different frequency bands.

Acknowledgement

The authors thank TOTAL for providing the data and for sponsoring Margherita Corciulo during this study. This study is part of the Whisper project (ERC Advanced Grant 227507).

References

Bakulin, A, A. Mateeva, K. Mehta, P. Jorgensen, J. Ferrandis, I. Shina Herold, and J. Lopez, 2007, Virtual source applications to imaging and reservoir monitoring: The Leading Edge, **26**, 732-740.

Bracewell, R. N., 1965, The Fourier transform and its applications: McGraw-Hill.

Brenguier, F., M. Campillo, C. Hadzioannou, N. M. Shapiro, R. M. Nadeau, and E. Larose, 2008, Postseismic relaxation along the San Andreas Fault at Parkfield from continuous seismological observation: Science, **321**, 1478-1481.

Brenguier, F., D. Clarke, Y. Aoki, N. M. Shapiro, M. Campillo, and V. Ferrazzini, 2011, Monitoring volcanoes using seismic noise correlations: Comptes Rendus Geoscience, doi:10.1016/j.crte.2010.12.010.

Draganov, D., K. Wapenaar, W. Mulder, J. Singer, and A.Verdel, 2007, Retrieval of reflections from seismic background-noise measurements: Geophysical Research Letters, **34**, L04305. doi:10.1029/2006GL028735.

Gabor, D., 1946, Theory of communication: Journal of the Institution of Electrical Engineers, **93**, 429-457.

Grêt, A., R. Snieder, R. C. Aster, and R. Kyle, 2005, Monitoring rapid temporal change in a volcano with coda wave interferometry: Geophysical Research Letters, **32**, L06304, doi:10.1029/2004GL021143.

Hadziioannou, C., E. Larose, O. Coutant, P. Roux, and M.Campillo, 2009, Stability of monitoring weak changes in multiply scattering media with ambient noise correlation: Laboratory experiments: Journal of the Acoustical Society of America, **125**, 3688-3695.

Hatchell, P., and K. Mehta, 2010, Ocean Bottom Seismic (OBS) timing drift correcting using passive seismic data: SEG Expanded Abstract, **29**, 2054. doi: 10.1190/1.3513249.

Hilbert, D., 1900, Mathematical Problems. Lecture delivered before the International Congress of Mathematicians in Paris, France.

Korneev, V., A. Bakulin, and J. Lopez, 2008, Imaging and monitoring with Virtual Sources on a synthetic 3D dataset from the Middle East: SEG Expanded Abstract, **27**, 3204. doi: 10.1190/1.3064011.

Poupinet, G., W. L. Ellsworth, and J. Frechet, 1984, Monitoring velocity variations in the crust using earthquake doublet: an application to the Calveras Fault, California: Journal of Geophysical Research, **89**, 5719-5731.

Roux, P, K. G. Sabra, W. A. Kuperman, and A. Roux, 2005, Ambient noise cross-correlation in free space: theoretical approach: Journal of the Acoustical Society of America, **117**, 79-84.

Roux, P., M. Wathelet, and A. Roueff, 2011, The San Andreas Fault revisited through seismic-noise and surface-wave tomography: Geophysical Research Letters, **38**, L13319, doi: 10.1029/2011GL047540.

Sabra, K. G., P. Roux, A. M. Thode, G. L. D'Spain, W. S. Hodgkiss, and W. A. Kuperman, 2005a, Using ocean ambient noise for array self-localization and self-synchronization: IEEE Journal of Oceanic Engineering, **30**, 338-347.

Sabra, K. G., P. Roux, and W. A. Kuperman, 2005b, Emergence rate of the time-domain Green's function from the ambient noise cross-correlation function: Journal of the Acoustical Society of America, **118**, 3524-3531.

Sabra, K. G., P. Roux, P. Gerstoft, W. A. Kuperman, and M. C. Fehler, 2006, Extracting coda arrivals from cross-correlations of long period scattered waves during the Mount St. Helens 2004 eruption: Geophysical Research Letters, **33**, L06313.

Schimmel, M., E. Stutzmann, and J. Gallart, 2011, Using the instantaneous phase coherence for signal extraction from ambient noise data at a local to a global scale: Geophysical Journal International, **184**, 494-506, doi: 10.1111/j.1365-246X.2010.04861.x.

Schuster, G. T., J. Yu, J. Sheng, and J. Rickett, 2004, Interferometric/ daylight seismic imaging: Geophysical Journal International, **157**, 838-852. doi: 10.1111/j.1365-246X.2004.02251.x.

Sens-Schönfelder, C., and U. C. Wegler, 2006, Passive image interferometry and seasonal variations of seismic velocity at Merapi Volcano, Indonesia: Geophysical Research Letters, **33**, L21302.

Shapiro, N. M., and M. Campillo, 2004, Emergence of broadband Rayleigh waves from correlations of the ambient seismic noise: Geophysical Research Letters, **31**, L07614.

Shapiro, N. M., M. Campillo, L. Stehly, and M. H. Ritzwoller, 2005, High-resolution surface-wave tomography from ambient seismic noise: Science, **307**, 1615-1618. doi:10.1126/science.1108339.

Snieder, R., A. Grêt, H. Douma, and J. Scales, 2002, Coda wave interferometry for estimating nonlinear behavior in seismic velocity: Science, **295**, 2253-2255.

Snieder, R., 2006, The theory of coda wave interferometry: Pure and Applied Geophysics, **163**, 455-473.

Snieder, R., 2007, Extracting the Green's function of attenuating heterogeneous acoustic media from uncorrelated waves: Journal of the Acoustic Society of America, **121**, 2637-2643.

Stehly, L, M. Campillo, and N. M. Shapiro, 2007, Travel time measurements from noise correlation: stability and detection of instrumental error: Geophysics Journal International, **171**, 223-230.

Weaver, R. L., and O. I. Lobkis, 2001, Ultrasonic without a source: Thermal fluctuation correlation at MHz frequencies: Physical Review Letters, **87**, 134301-134304.

Weaver, R. L., and O. I. Lobkis, 2004, Diffuse fields in open systems and the emergence of the Green's function: Journal of the Acoustic Society of America, **116**, 2731-2734.

Weaver, R. L., C. Hadziioannou, E. Larose, and M. Campillo, 2011, On the precision of noise correlation interferometry: Geophysical Journal International, **185**, 1384-1392.

Yao, H. R., R. D. van der Hilst, and M. V. de Hoop, 2006, Surface-wave array tomography in SE Tibet from ambient noise at two-station analysis – I. Phase velocity maps: Geophysical Journal International, **166**, 732-744, doi/10.1111/j.1365-246X.2006.03028.x.

Figures

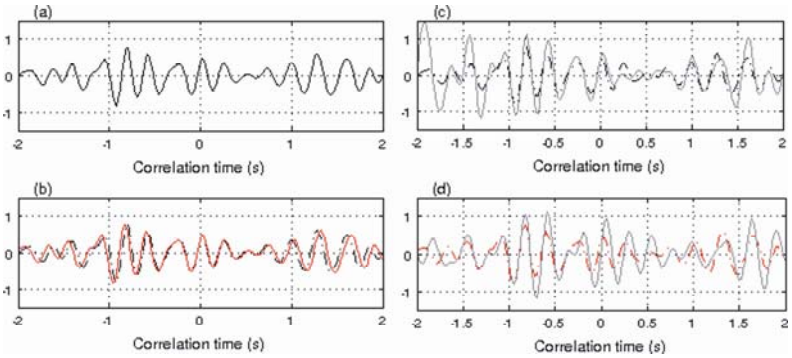

Figure 1: Synthetic signals generated using a 50 Hz sampling frequency and a [2-5 Hz] band-pass filter. a) Reference signal; b) Stretched signal (red line) and reference signal (dashed black line); c) Noised reference signal (gray line) and reference signal (dashed black line); d) Noised stretched signal (gray line) and stretched signal (dashed red line).

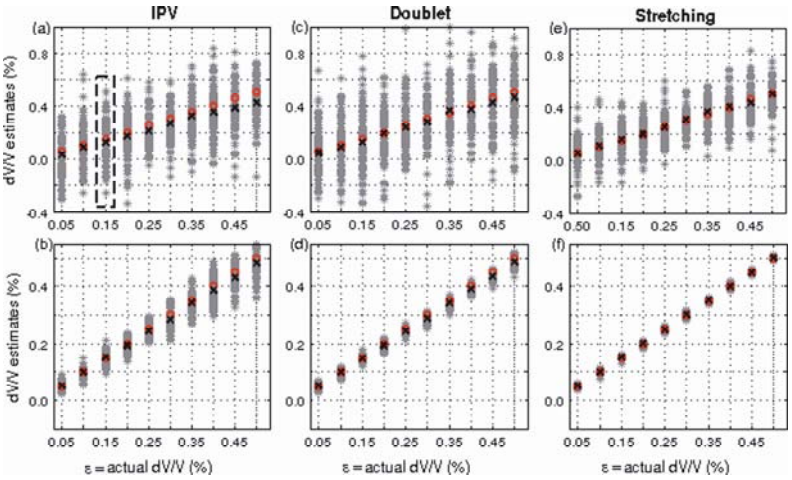

Figure 2: Statistical analysis of the dV/V estimates *versus* ε, the actual dV/V stretching of the reference synthetic signal. For each ε, 1000 different realizations of the reference signal were tested. The dV/V estimation is performed with the IPV technique in (a) and (b), the doublet (c) and (d) and the stretching algorithm (e) and (f). The monitoring results were obtained using synthetic data computed with SNR = 5 for (a), (b) and (c), and SNR = 100 for (d), (e) and (f). In each plot, the red circles correspond to the ε values and the black crosses are the mean values of the Gaussian fit (see Figure 3a). The black dashed box in (a) corresponds to the dV/V distribution shown in Figure 3a.

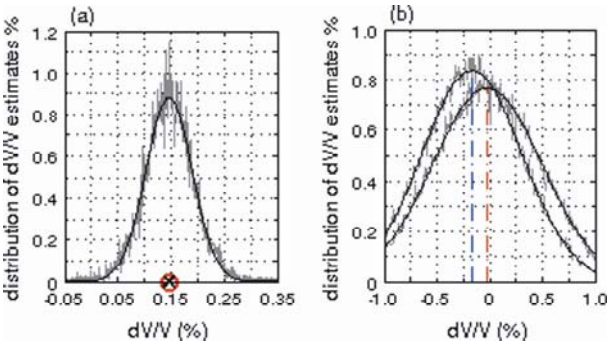

Figure 3: Statistical distribution of the dV/V estimates for the IPV technique (gray lines). The black lines correspond to the Gaussian fit. (a) Distribution of the N = 1000 dV/V estimates for the synthetic test that corresponds to the gray dashed box in Figure 2a, with SNR = 5. Black cross: mean value of the Gaussian fit; red circle: ε value. (b) Distribution of the N ~70000 dV/V estimates for the experimental dataset at two different acquisition times (Figure 7a, red and blue arrows), with SNR = 2.76. The dashed vertical lines correspond to the means of the Gaussian fits retrieved at each acquisition time (colors as for Figure 7a).

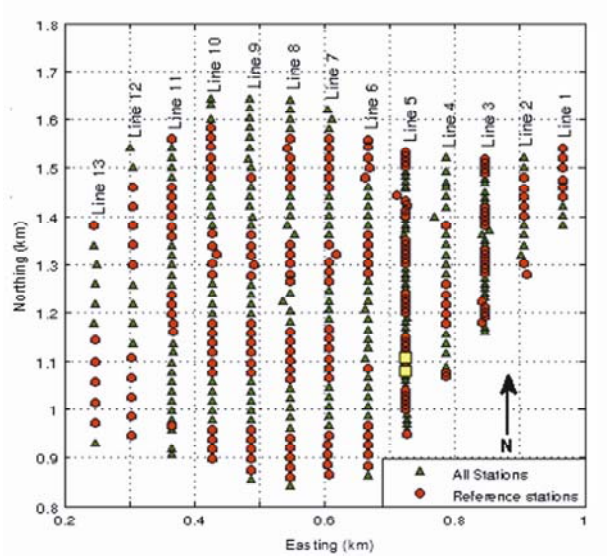

Figure 4: Data acquisition geometry. Green triangles, location of the 397 vertical-component geophones. Red spots, subset of geophones used to compute the cross-correlation signals (reference stations). Yellow squares, the two geophones used to built the time-evolving cross-correlated signals in Figure 6 (stations #125 and #128, separated by a 30-m distance). The network dimension is 800 m × 900 m.

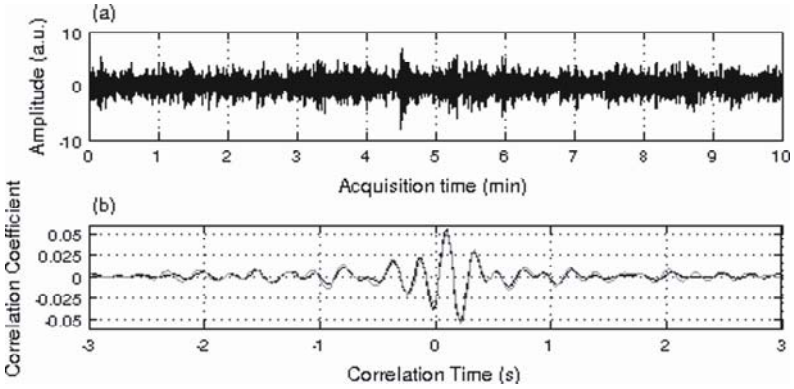

Figure 5: (a) Plot of 10 mins of noise data acquired by geophone #125 located on line #5 (see Figure 4), pre-filtered in the [2-5 Hz] frequency band. (b) One CCF obtained for a 10-min noise window between stations #125 and #128 (gray line) and the same CCF averaged over the five acquisition days (black line).

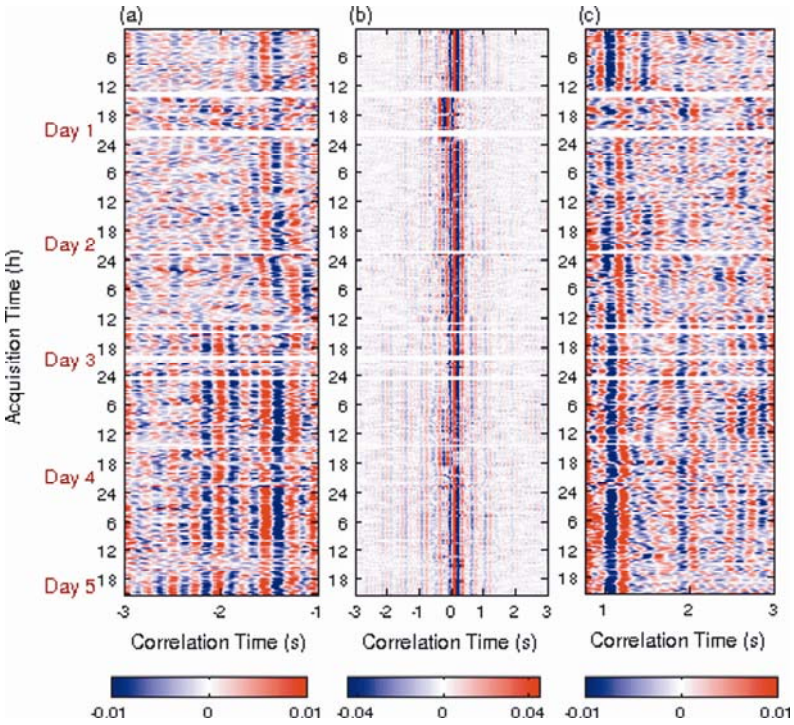

Figure 6: Temporal evolution of the CCF between stations #125 and #128 (Figure 4, yellow squares) computed on successive 10-min noise windows, pre-filtered between 2.0 Hz and 5.0 Hz. The X axis is the correlation time in seconds. The Y axis corresponds to the acquisition time in hours. (a), (c) Zooms into the late parts of the CCF in the time intervals [-3s, -1s] and [1s, 3s], respectively. (b) Plot of the whole CCF between -3s and 3s.

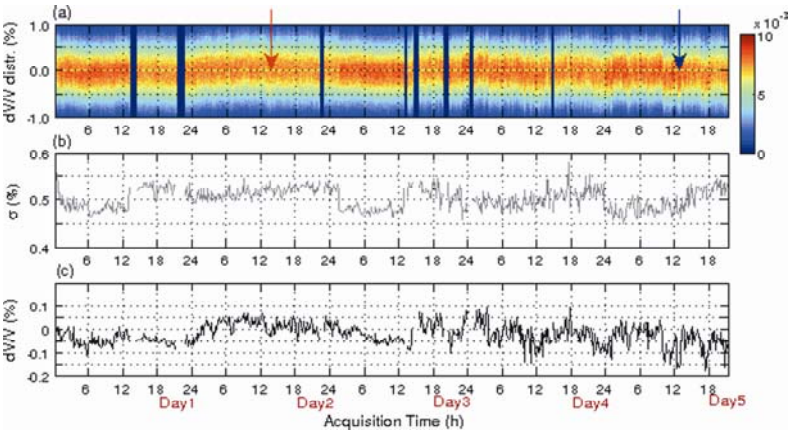

Figure 7: (a) Temporal evolution of the statistical distribution of the dV/V estimates through the IPV method. Dark blue intervals, missing or incorrect data. Red and blue arrows, selected time windows used in Figure 3b. (b) Temporal evolution of the standard deviation (σ) of the dV/V distribution obtained from the Gaussian fit. (c) Temporal evolution of the mean of the dV/V distribution from the Gaussian fit.

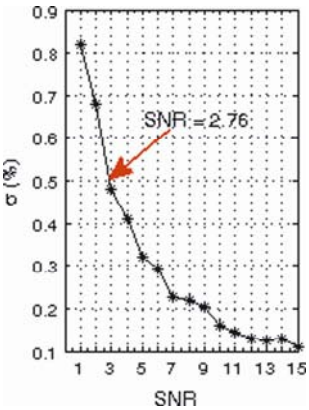

Figure 8: Standard deviation (σ) of the Gaussian fit as a function of the SNR of the CCF for the synthetic tests obtained with the IPV results (see Figure 3). Red arrow, position of the average experimental result (SNR = 2.76) along the σ *vs* SNR plot.

Tables

Computing time	Monitoring algorithm		
	IPV	**Stretching**	**Doublet**
Absolute (s)	0.00616	0.07412	0.13176
Relative (to IPV)	1:1	1:12	1:21

Table 1: Comparison of the computation times (relative and absolute) between the doublet, stretching and IPV monitoring algorithms for one CCF.